Supercritical flow at abrupt expansions

W. H. Hager, PhD, and S. K. Mazumder, PhD

Proc. Instn Civ. Engrs Wat., Marit. & Energy, 1992, **96**, Sept., 153–166

Paper 9894

Written discussion closes 17 November 1992

■ **Abrupt channel expansions with supercritical approach flow are important elements of outlets and spillways. An experimental study was carried out, in which both the free surface and the velocity field were accounted for. Similarity is found for the flow surface profiles, whereas the velocity field is affected by a significant scale effect involving the Reynolds number. A non-dimensional approach is used for further investigation of the axial and wall surface profiles. The flow field is illustrated by typical photographs, and a generalized design method is presented. The fundamental flow configuration in an abrupt expansion is analysed, and the results may serve as a basis for improving supercritical expansion flow.**

Notation

Quantities with overbar denote cross-sectional averages.

- A cross-sectional area
- B channel width
- F Froude number
- g gravitational acceleration
- h flow depth
- k_s equivalent roughness height
- K Manning–Strickler roughness coefficient
- L length
- n number of data
- q discharge per unit width
- Q discharge
- R Reynolds number
- R_h hydraulic radius
- S_o bottom slope
- S_f friction slope
- T_t lateral momentum transfer coefficient
- u streamwise velocity component
- v transverse velocity component
- V absolute value of velocity
- W_f waviness factor
- x streamwise coordinate
- $X = (x/b_o^{-1})\,F_o^{-1}$ dimensionless streamwise coordinate
- X_B boundary coordinate
- y transverse coordinate
- Y relative flow depth
- Y_B boundary coordinate
- α Coriolis coefficient
- β expansion ratio
- θ angle of streamline
- σ standard deviation
- τ relative location along wall
- υ kinematic viscosity
- ζ boundary curve parameter

Subscripts

- a axis
- b flow boundary
- B channel boundary
- i impingement
- m minimum
- M maximum
- o approach
- p tangency point
- s shock front
- t transition
- T transverse
- w wall
- 0 scaling quantities
- 1 quantities upstream from shock
- 2 tailwater quantities

Introduction

Abrupt expansions form one type of open channel transition, e.g. a transition structure of a spillway, a flood relief canal or a bottom outlet gallery as a part of a hydraulic scheme. The flow pattern in such expansions is complex, and knowledge of the hydraulic performance and design procedures is poor.

2. Although it is generally known that every disturbance of supercritical flow creates cross or shock waves, the actual information on the shock wave pattern in channel expansions is incomplete. For transitions from steep to less steep spillways, one would typically expand the channel to obtain prescribed tailwater flow depth. A conventional design would, however, imply a prismatic channel with increased side wall height, the generation of shock waves thus being suppressed.

3. This Paper aims at responding to two basic questions.

(*a*) What is the flow pattern downstream of an abrupt expansion?

(*b*) What are the design quantities of the abrupt expansion?

Review

4. The first and still most significant contribution to supercritical flow in horizontal channel expansions is attributable to Rouse *et al.*[1] By dimensional analysis, the free surface $h = h(x, y)$ downstream from an abrupt expansion depends on the approach width b_o, the approach flow depth h_o and the approach Froude number $F_o = Q/(gb_o^2 h_o^3)^{1/2}$ (Fig. 1). Quantities x and y are the streamwise and transverse coordinates with origin at the axis of a symmetrical expansion section. For pure gravity flow, the relative surface of flow may be expressed as

$$\frac{h}{h_o} = f_1\left(\frac{x}{b_o}, \frac{y}{b_o}, F_o\right) \qquad (1)$$

W. H. Hager, Versuchsanstalt für Wasserbau, Hydrologie und Glaziologie, ETH-Zentrum, Zurich

S. K. Mazumder, Department of Civil Engineering, Delhi College of Engineering, Delhi; formerly Visiting Professor, Laboratoire de Constructions Hydrauliques DGC, EPFL, Lausanne

The effect of b_o/h_o was shown to be of secondary order and neglected. Also, the effect of Froude number could be included in a modified streamwise coordinate $X = (x/b_o)F_o^{-1}$ to read

$$\frac{h}{h_o} = f_2\left(X, \frac{y}{b_o}\right) \tag{2}$$

The surface downstream from a horizontal abrupt expansion may therefore be represented with a three-parameter plot.

5. The second part of the paper by Rouse *et al.*[1] deals with a continuous wall geometry to reduce the formation of shock waves in a finite width expansion. The boundary curve $y_b(x)$ enclosing some 90% of discharge is

$$\frac{y_b}{b_o} = \tfrac{1}{2}(1 + \zeta X^{3/2}) \tag{3}$$

in which $\zeta = 1$. Separation from the expanding curve may be inhibited if $\zeta = 1/4$. From the tangency point up to the end of expansion, a receding curve $Y_B(X_B)$ is defined. The complete length of transition L_t may be expressed for expansion ratios $\beta = b/b_o \leqslant 5$ as

$$\frac{L_t}{b_o F_o} = 1 + 3{\cdot}25(\beta - 1) \tag{4}$$

Further, the position of the tangency point from the origin is

$$\frac{L_p}{b_o F_o} = 0{\cdot}7\beta \tag{5}$$

in which $X_B = (x - L_p)/(L_t - L_p)$ and $Y_B = (y - y_p)/(\beta b_o/2 - y_p)$, where y_p is the transverse location of the tangency point according to equation (3). The transition curve from the point of tangency to the end of transition may be approximated from Rouse *et al.*'s curve as

$$Y_B = \sin(90^\circ X_B), \quad 0 \leqslant X_B \leqslant 1 \tag{6}$$

The Rouse transition curve is quite long and increases according to equation (4) linearly with F_o. For $\beta = 3$ and $F_o = 4$, the relative length is $L_t/b_o = 30$; whereas for $F_o = 10$, $L_t/b_o = 75$. Until now, no serious attempt to reduce the length of transition curve has been made.

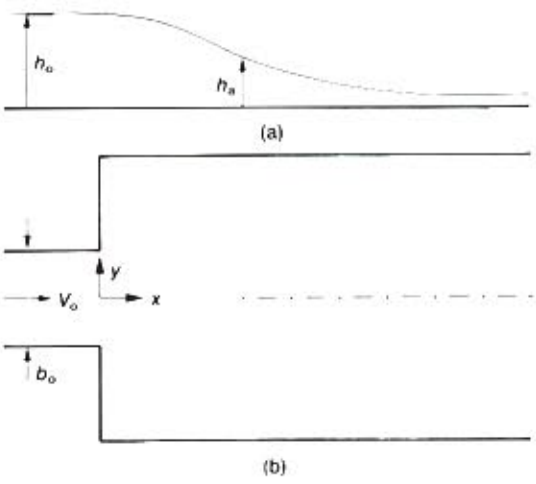

Fig. 1. Abrupt channel expansion, definition of flow: (a) longitudinal section; (b) plan view

6. Additional studies were conducted by Guenzel,[2] Sherenkov,[3] and Koch.[4] A simplified theory was given by Engelund.[5] When $\bar{b}$ and $\bar{h}$ denote the average cross-sectional width and height of flow, and S_o and S_f the bottom slope and friction slope respectively, the streamwise momentum equation reads

$$\frac{\mathrm{d}}{\mathrm{d}x}\left(\frac{1}{2}\bar{b}\bar{h}^2 + \frac{Q^2}{g\bar{b}\bar{h}}\right) = \bar{b}\bar{h}(S_o - S_f) \tag{7}$$

The corresponding lateral component of momentum equation may be expressed as

$$\frac{1}{2}\bar{h}^2 = \frac{\mathrm{d}}{\mathrm{d}x}\left(\frac{1}{2}\frac{Q^2}{\bar{b}\bar{h}}\frac{\mathrm{d}\bar{b}}{\mathrm{d}x}\right) + \bar{b}\bar{h}\bar{S}_f\left(\frac{1}{2}\frac{\mathrm{d}\bar{b}}{\mathrm{d}x}\right) \tag{8}$$

The term on the left-hand side accounts for the axial pressure force. The first term on the right-hand side is the component of lateral momentum, and the second term describes the lateral component of bed shear stress. For further analysis, the friction slope $\bar{S}_f$ was expressed with the Manning formula. A similarity analysis yielded three scaling lengths h_0, b_0 and x_0 as a function of discharge and roughness value. Preliminary experiments showed that unique functions $\bar{h}/h_0(x/x_0)$ and $\bar{b}/b_0(x/x_0)$ existed, independent of the approach Froude number and the bottom slope.

7. The first numerical modelling of flow in a gradual Rouse-type expansion was executed by Bellos *et al.*[6] The governing set of shallow water equations was transformed in a square grid net to simplify the computations along curved boundaries. Then the McCormack two-step scheme was used to determine the free surface for an approach Froude number $F_o = 2$. The comparison along the centre-line with the experimental data was fair and good along the wall and the intermediate section between axis and wall profiles.

8. The review of literature indicates that supercritical flows in expansions are not actually covered by extended experiments by means of which numerical computations could be checked. One objective of the present study is to fill this gap. A second objective is to study both the free surface and the velocity field of the abrupt expansion as a basis for further improvement of flow.

Experimental installation

9. The experiments were conducted in a channel used previously by Bremen.[7] The water was led into a tank 3 m in height, with a square surface of 2 m × 2 m. Its outflow was improved with two porous walls located 1 m and 0·5 m upstream from the outflow section, and a streamlined gate extended by a tailwater cover to guide the flow into the 0·50 m wide and

1·2 m long approach channel. The origin of the coordinate system was located at the axis of the expansion section. At $x = 0$, the channel expanded abruptly to the tailwater channel of width $b_2 = 1{\cdot}5$ m. The main experiments were therefore conducted in a channel with an expansion ratio $\beta = b_2/b_o = 3$. Additional experiments for $\beta = 2$ and $\beta = 5$ were made by inserting channel walls. The flow in this 8 m long channel could be submerged with a tailwater flap gate. The channel bottom and the right-hand side side wall were made of PVC, whereas the left side was made of glass to permit observation.

10. The installation permitted discharges up to 270 ls^{-1} and maximum velocities of up to 7 ms^{-1}. The gate could be lifted to a maximum of 0·20 m. During the experiments to be described, three approach flow depths were considered, namely $h_o = 24$ mm, 48 mm and 96 mm. The approach Froude numbers were $F_o = 1, 2, 4, 6$ and 8. Therefore, scale effects could also be analysed.

11. The observation of flow included the free surface $h(x, y)$, as well as the magnitude $V(x, y)$ and the direction of velocity field $\theta(x, y)$. The flow depth h was measured with a point gauge to the nearest mm. On account of the high velocity flow, an electrical contact method was used. Repetitive observation showed that the errors are confined to ± 1 mm.

12. The direction of streamlines was observed with a flow direction probe. A flag-type Plexiglas plate, 30 mm long and 15 mm high, mounted on a metal pole transmitted the local value of angle θ to the top of suspension rod where the angle could be read to the nearest degree. Then the miniature propeller meter of 8 mm internal dia. was set in the direction of flow as previously established. Preliminary observations revealed that the variation of angle and velocity in the vertical direction is small, and therefore negligible. Apart from the boundary layer, and the domains close to the expansion section, the flow may be regarded as almost plane. To obtain a two-dimensional flow field, both the angle meter and the propeller were located at half of the local flow depth above the bed. Special air deflection devices inhibited air entrainment to the probes.

13. For flow depths smaller than 25 mm, the propeller probe could not be set in the flow without aeration, in which case a modified Pitot tube was used for total head readings. To dampen the water column fluctuations, a Scotch adhesive tape with a central cut was mounted on the glass tube entrance. The modified Pitot tube proved to be a simple and most effective device, as velocities up to 6·5 ms^{-1} down to flow depths of 15 mm could be observed.

14. One of the reasons that supercritical flow in channel expansions has received only scarce attention to date is the difficulty inherent in the methods of measurement. A second problem is the precision with which a large model should be finished. In the present case, variations in the bottom from the horizontal were ± 1 mm. A third difficulty was the uniformity of approach flow for large flow depths h_o and large discharges Q.

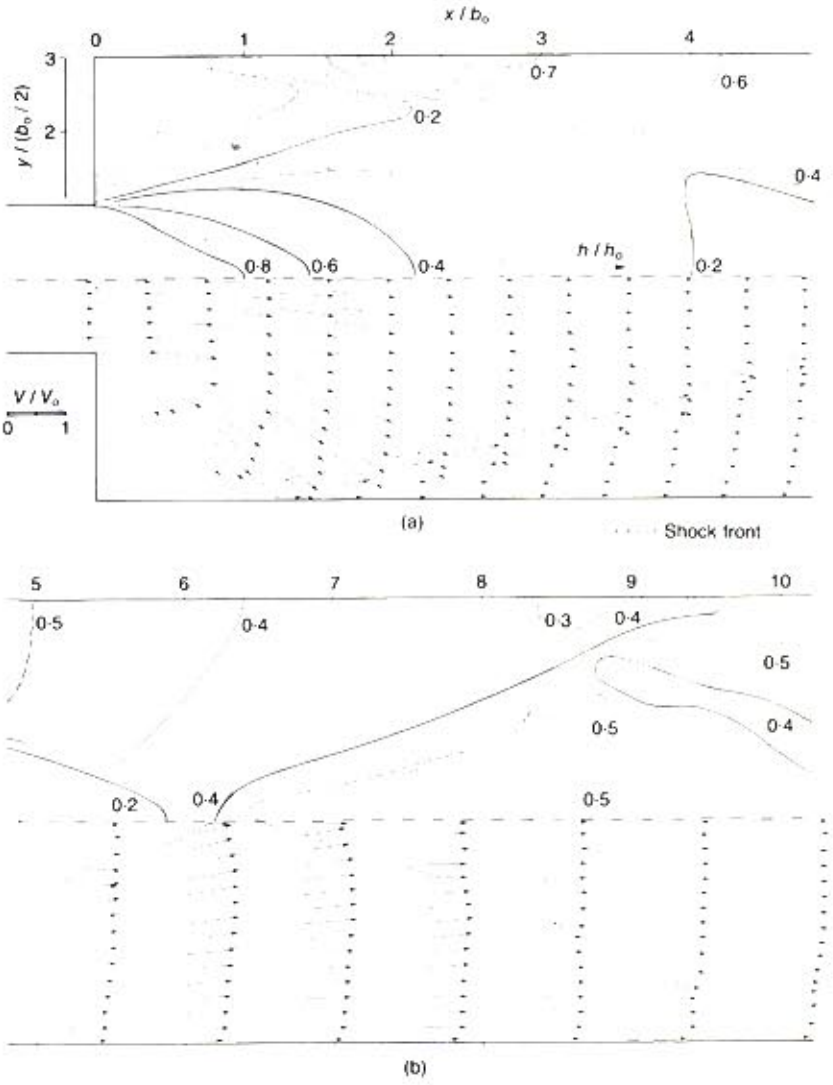

Fig. 2. Flow in abrupt expansion for $h_o = 96$ mm, $F_o = 2$. Contour lines h/h_o (top), and velocity field (bottom) for: (a) $0 < x/b_o < 4{\cdot}8$; (b) $4{\cdot}8 < x/b_o < 10$

Experimental results

15. The data on typical figures are shown as surface contours on the upper portion and as velocity distributions on the lower portion, with respect to the axis of symmetry. The scalings are b_o for length, h_o for flow depth and $V_o = (gh_o)^{1/2} F_o$ for velocity. All results in this section refer to an expansion ratio of $\beta = 3$.

16. In Fig. 2, the demarcation line between flow and corner deadwater downstream from the expansion section to the impingement point, as well as the shock front further downstream, is included as a dotted curve. The flow is seen to spread almost linearly, and full expansion has occurred at $x_i/b_o = 0{\cdot}85$. Then the shock front divides the flow into a disturbed wall domain and an undisturbed central core. In the latter, the flow continues to spread up to the

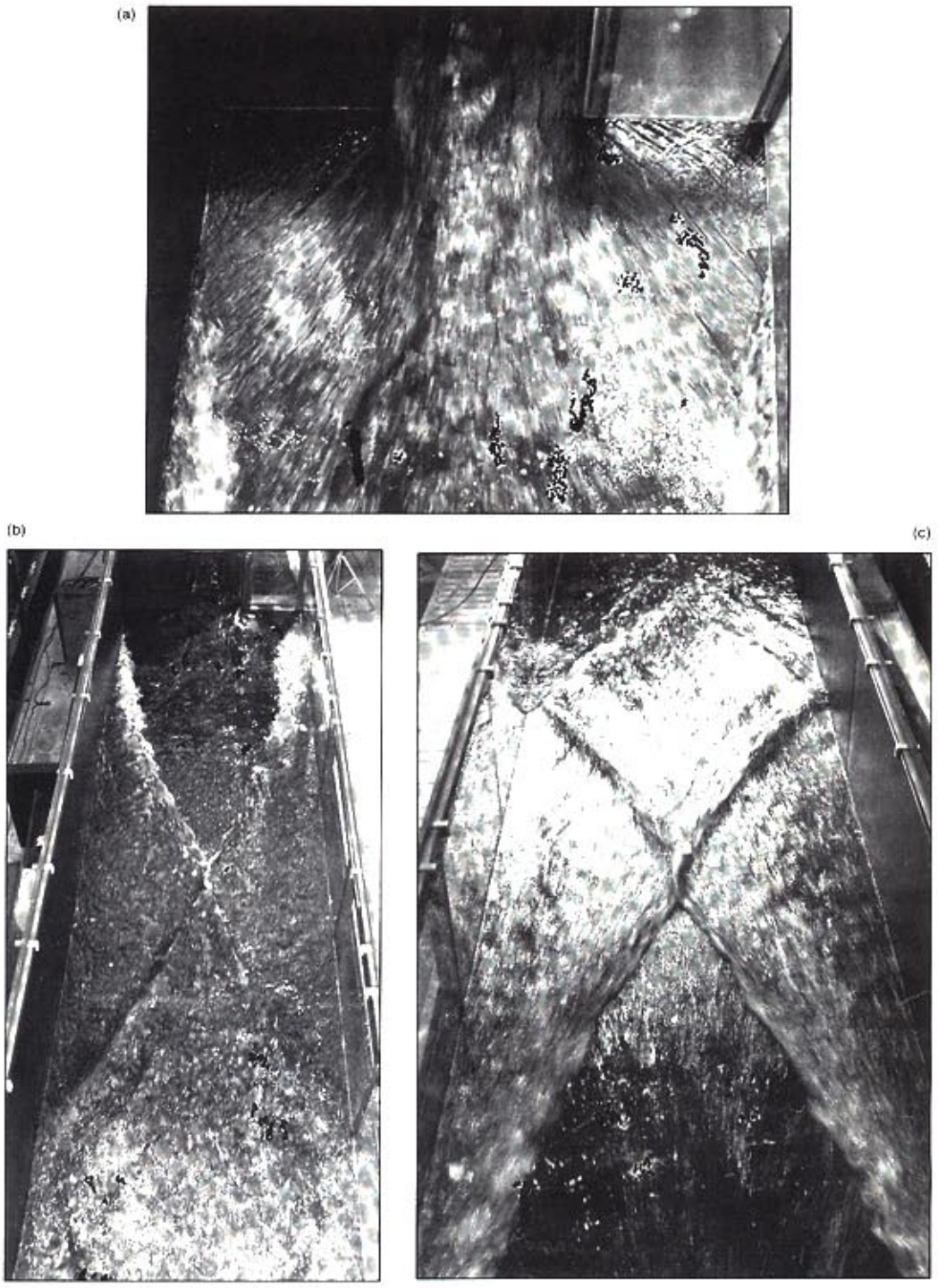

Fig. 3. Flow with $h_o = 96$ mm, $F_o = 2$ and $\beta = 3$

Table 1. Typical values along shock front and comparison with conventional approach

x: m	h_1: mm	F_1: —	θ_{1e}: degrees	θ_{1p}: degrees	h_{2e}: mm	h_{2p}: mm
1·2	30	0	—	—	80	
1·6	30	2·23	16	22	100	57
2·0	35	3·24	15	15	150	77
2·4	50	3·87	15	13	190	121
2·8	85	4·04	14	12	220	203
3·2	100	3·96	14	12	310	236
3·6	125	3·57	12	13	370	257
4·0	135	3·27	10	15	405	244

shock front, whereas a hill-shaped zone forms along the wall with maximum $h_M/h_o = 0{\cdot}77$ at $x_M/b_o \cong 2{\cdot}4$. The angle of shock front is initially about 11°, but increases to 21° at the point where it crosses the channel axis ($x_a/b_o = 6{\cdot}2$). Beyond this point, the flow in the wall domain decreases further in depth, while a complicated wave pattern occurs in the central domain. This must be attributed to the small local Froude numbers slightly in excess of 1. The second portion of shock front impinges the wall at $x/b_o = 9{\cdot}5$. In this Paper, attention is focused on the domain between the expansion section up to the first crossing of shock waves, i.e. to the end of central core flow.

17. Figure 3(a) shows the transition from approach to tailwater channels in the domain of the expansion section. The local variation of flow parameters in this domain is significant, and a two-dimensional approach would be only a poor approximation close to the sides of the expanding stream. Also visible is the impingement of flow on the side walls and the resulting shock front. Table 1 gives the flow depth h_1, the Froude number $\boldsymbol{F}_1$, and the streamline directions θ_1 relative to the channel axis in front of the shock front at different locations x. Also given are the local values of measured angle θ_{1c} and flow depth h_{2c} beyond the shock. It is seen in this typical case that both $\boldsymbol{F}_1$ and h_1 increase to a maximum and then decrease slowly. The angle of streamline θ_1 decreases steadily. The prediction of both θ_{1p} and h_{2p} are rather poor as compared with observations. This was found already by Hager *et al.*,[8] and must be attributed to non-linear effects. As a conclusion, numerical predictions based on the shallow water equations (e.g. Ellis and Pender[9]) will deviate considerably from observations, owing mainly to the neglect of streamline curvature. Therefore, this study concentrated on experiments, and the results may serve as a database for more refined numerical models.

18. Figure 3(b) shows an overall view at the expansion section, while Fig. 3(c) relates to the complete flow field. The wave pattern downstream of the first axial reflection may be seen from Fig. 3(b).

19. The second series of photographs (Fig. 4) refers to $h_o = 96$ mm and $\boldsymbol{F}_o = 4$. Compared with the run with $\boldsymbol{F}_o = 2$, it is characterized by much sharper shock fronts and the absence of undular oblique jumps. Fig. 4(a) and (b) shows upstream and downstream views, while Fig. 4(c) gives an impression of the high velocity flow. Fig. 4(d) refers to the expanding flow beyond the expansion section.

20. The flow features of $\boldsymbol{F}_o = 8$ could be explored only with $h_o = 48$ mm, since the head for larger gate opening was not available. Fig. 5 shows an analogue to Fig. 2 except that the entire flow seems to be stretched. The available length of tailwater channel was just sufficient to observe the flow up to the first axial reflection.

21. Compared with Fig. 2, no wavy surface pattern may be seen in Fig. 5 for high $\boldsymbol{F}_o$. Also, the contour curves are much sharper, and the assumption of hydrostatic pressure distribution seems now to be satisfied. With regard to the distribution of velocities, the central core is characterized by an almost uniform velocity. Closer to the side walls, the velocity decreases significantly. The rate of decrease is inversely proportional to the distance from the expansion section. Beyond the impingement point ($x_i/b_o = 2{\cdot}4$), the velocity increases in the shock domain. At $x/b_o \simeq 8$, there are almost two co-flowing currents: one in the inner core domain; the other in the outer wall domain. The velocity distribution in the two domains is almost uniform and there is a distinct difference velocity ΔV between inner and outer domains. The difference of velocity ΔV decreases eventually to zero at the location $x/b_o \simeq 12{\cdot}4$. Further downstream, the velocity in the core domain is reduced considerably to the axial reflection point ($x/b_o \simeq 15{\cdot}4$), while the velocity in the outer domain remains approximately constant. Table 2 gives an overview on the various experiments which were conducted at the abrupt expansion.

22. Figure 6 shows some details of shock waves, including the axial crossing, the overlapping of core flow and wall flow domains, and reflection at the wall.

Generalization of results

23. According to Rouse *et al.*,[1] the effect of Froude number may be included in the streamwise coordinate as $X = (x/b_o)\boldsymbol{F}_o^{-1}$. In order to test this presumption, and to simplify the discussion of results, this approach was analysed further.

24. Figure 7(a) shows the *axial surface profile* $Y_a = h_a/h_o$ as a function of X. Up to the point of axial shock wave reflection, similarity exists between the curves $Y_a(X)$ for $h_o = 48$ mm and 96 mm, and $2 \leqslant \boldsymbol{F}_o \leqslant 8$, and it may be expressed as

$$Y_a = 0{\cdot}2 + 0{\cdot}8 \exp(-X^2) \tag{9}$$

Note that the location of first axial shock wave reflection does not coincide. For small h_o and large $\boldsymbol{F}_o$, it is located closer to the expansion section than for larger h_o and smaller $\boldsymbol{F}_o$. This scale effect must be attributed mainly to viscosity, as is shown below. Also, the run with $h_o = 24$ mm ($\boldsymbol{R}_o = 0{\cdot}20 \times 10^6$) deviates considerably from the general curve, except for $0{\cdot}6 \leqslant X \leqslant 1$.

25. In Fig. 7(b), the *wall surface profile* $Y_w = h_w/h_o$ is plotted as a function of dimensionless distance X. Apart from $h_o = 24$ mm, similarity occurs, except close to the expansion section at the dead-water zone, where the stag-

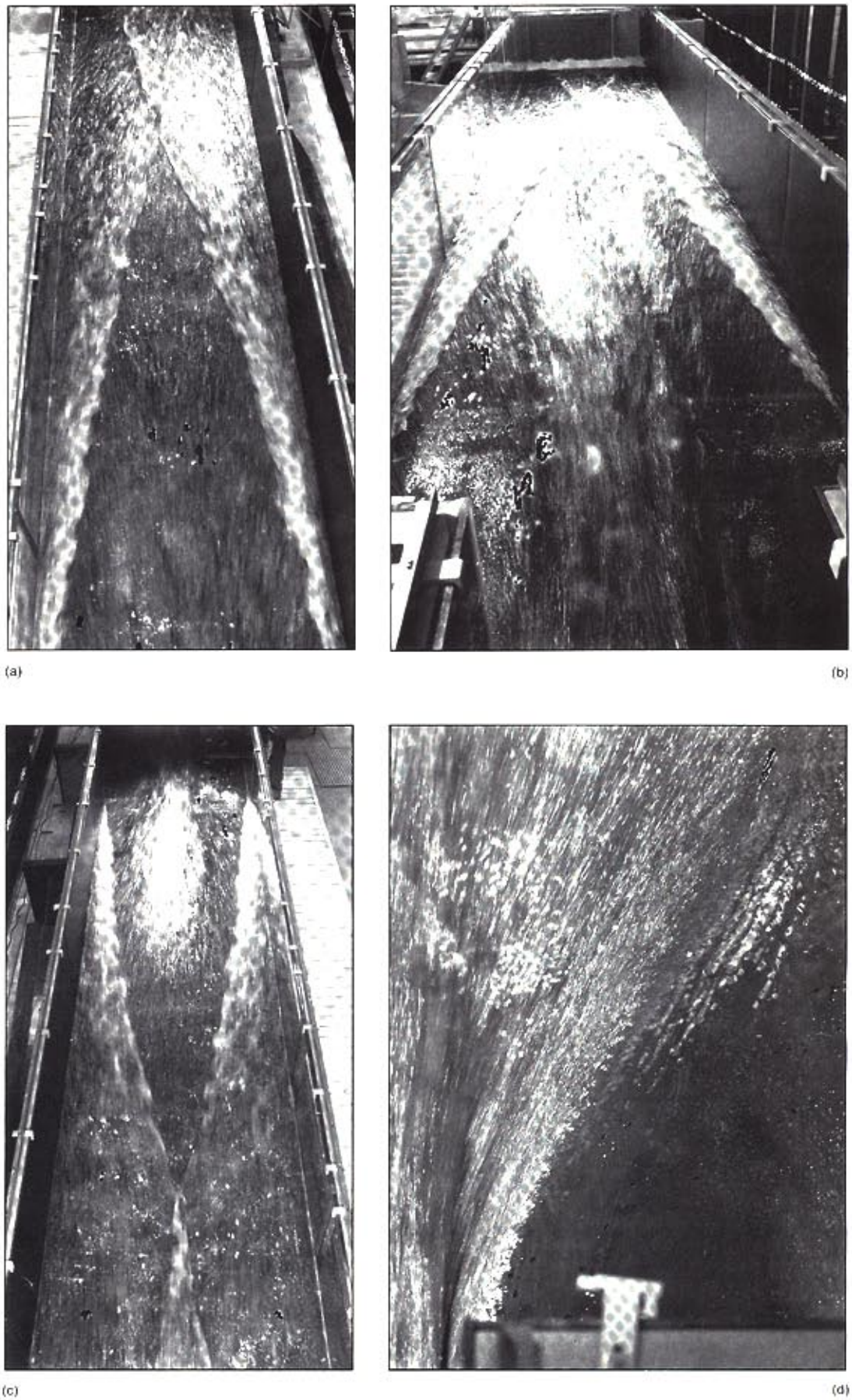

Fig. 4. Flow with $h_o = 96$ *mm,* $F_o = 4$ *and* $\beta = 3$

Table 2. Experiments conducted in abrupt expansion with $\beta = 3$; approach Reynolds number $R_o = 4R_h V_o/\nu$ based on kinematic viscosity $\nu = 1{\cdot}3 \times 10^{-6}$ m^2 s^{-1}

Run	h_o: mm	F_o	R_o
1	48	4	$0{\cdot}34 \times 10^6$
2	48	6	$0{\cdot}51 \times 10^6$
3	48	8	$0{\cdot}68 \times 10^6$
4	96	2	$0{\cdot}41 \times 10^6$
5	96	4	$0{\cdot}83 \times 10^6$
6	24	6	$0{\cdot}20 \times 10^6$

nant water depth depends on surface tension. In the domain $0 \leqslant X \leqslant 1/3$, $Y_w = 0$ may practically be set in a large channel, and more downstream for the wall profile

$$Y_w = 0{\cdot}81\tau \exp(1 - \tau) \qquad (10)$$

Herein, the scaling $\tau = X - 1/3$ accounts for a horizontal shift of the wall profile curve. The *maximum* wall depth $Y_{wM} = 0{\cdot}81$ occurs at location $\tau = 1$, i.e. $X_M = 4/3$. This important finding indicates that the wall height in the expanding channel portion has to be at least 81% of the approach depth h_o, independent of the approach Froude number. Its location is $X_M = (4/3)b_o F_o$, thus linearly variable with F_o.

26. In a typical application, the approach flow in a wide rectangular chute is nearly uniform and may be described with the Manning–Strickler formula

$$q = KS_o^{1/2} h_o^{5/3} \qquad (11)$$

where q is the discharge per unit width, S_o is the bottom slope, and h_o is the uniform approach flow depth. Therefore, the Froude number is equal to $F_o = KS_o^{1/2} h_o^{1/6} g^{-1/2}$, where g is the gravitational acceleration and thus almost independent of h_o. As a result, the wall height has to be determined from the maximum approach depth h_o, while the location x_M of maximum depth is practically constant. An additional freeboard is needed to account for spray formation and other simplifications accounted for.

27. The transverse surface profile $Y_T(y)$ for a particular value of X, where $Y_T = h/h_*$, is shown in Fig. 8 for $X = 0{\cdot}25$ and $0{\cdot}75$. Again, a reasonable similarity may be noted which improves as $X \to 0$. Fig. 9 shows the average curves $Y[y/(b_o/2)]$ for various X up to the domain of shock front. Accordingly, the free surface in the core domain may be described completely by a function in which the streamwise and transverse effects are split. The Froude similarity law seems to be applicable for $R_o > 0{\cdot}3$ to $0{\cdot}4 \times 10^6$.

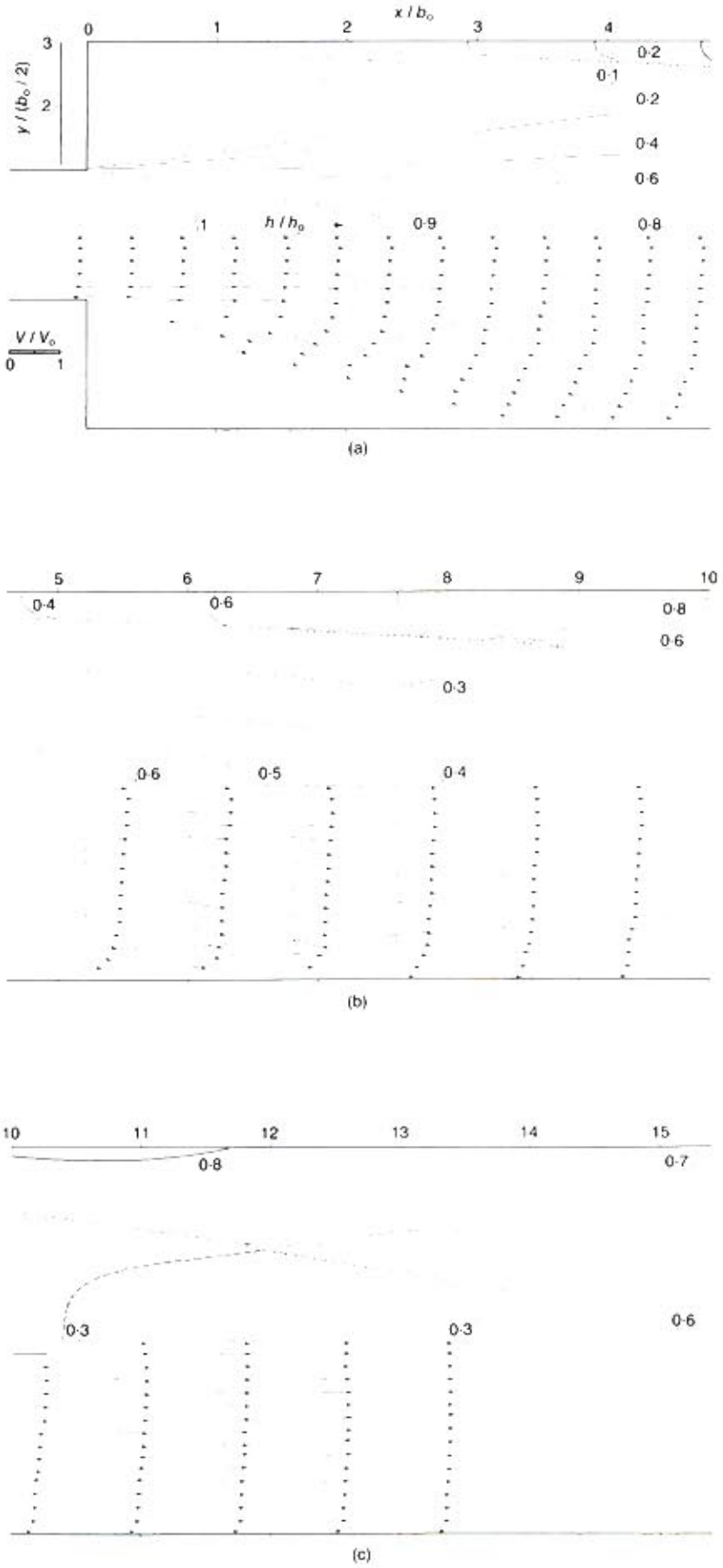

Fig. 5. Flow in expansion for $h_o = 48$ mm, $F_o = 8$ and $\beta = 3$ (for notation, see Fig. 2)

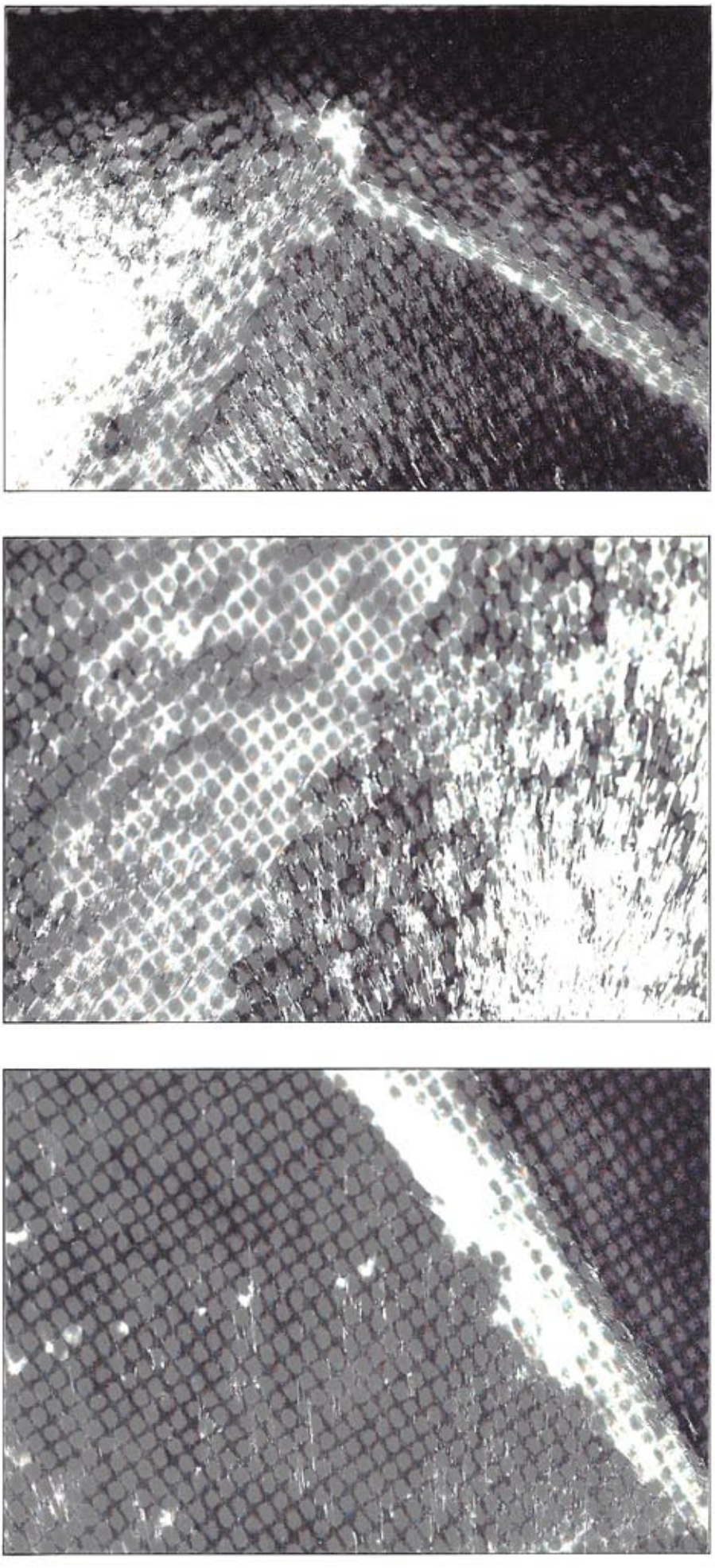

Fig. 6. Details of shock waves

Velocity distribution

28. The axial velocity plot V_a/V_o as a function of dimensionless coordinate X is shown in Fig. 10(a). Compared with Fig. 7(a), significant scale effects are now present, which are due mainly to viscosity, and, to a smaller extent, to boundary roughness (the equivalent roughness height is estimated to 0·1 mm, as the PVC coating was partly slightly damaged). The decay of streamwise velocity clearly increases both as h_o decreases and F_o increases. For $F_o = 2$, the axial velocity is almost preserved up to $X = 2$, while 90% of V_o occurs for $F_o = 4$ and $h_o = 96$ mm. Up to the point of axial shock wave reflection, the gradient of the function $V_a(x)$ is almost constant, and may be estimated from the approach flow gradient.

29. The velocity profile along the wall is plotted in Fig. 10(b). Here, 'along the wall' means outside of the wall boundary layer, i.e. at $y = 72$ cm. The profiles start abruptly from 0 at $X \simeq 0{\cdot}4$ to a more or less constant value for $0{\cdot}8 < X < 3$. Again, the constant value increases with h_o and F_o^{-1}. The run with $h_o = 24$ mm has again a strong scale effect as chocking occurs for $X > 1{\cdot}3$.

Location of shock fronts

30. The location of shocks was defined as follows. According to Ippen and Harleman,[10] a shock front is not really a standing vertical-wave, but rather its front is S-shaped in section and may become undular, depending on the approach Froude number F_1. Hager *et al.*[8] have further explored the transverse geometry of a shock front for $F_1 \geqslant 2{\cdot}8$. Undulations of a shock resulting from wall reflection may or may not occur, depending on the location relative to the origin of disturbance.

31. In the present case, the general pattern of flow was two-dimensional, although there were spatial flow features close to the expansion section and at domains of shock reflections. The location of shock was therefore defined where the overlapping of tailwater flow over incident flow started. In general, the shock front fluctuated about ± 1 cm, and fluctuations grew with increasing distance from the expansion section. Although not a real shock, the demarcation line between core flow and corner stagnation was also observed. Thus a continuous line may be plotted, starting downstream from the approach side wall and indicating the boundary between core domain and perturbed wall domain.

32. Figure 11 shows a generalized plot of shock location $Y_s = y_s/(b_o/2)$ as a function of longitudinal coordinate X. Significant effects of scale may again be seen beyond the first reflection point, particularly for $h_o = 24$ mm. Also, the data for $h_o = 48$ mm depart from those for $h_o = 96$ mm. Included in Fig. 11 as a solid curve

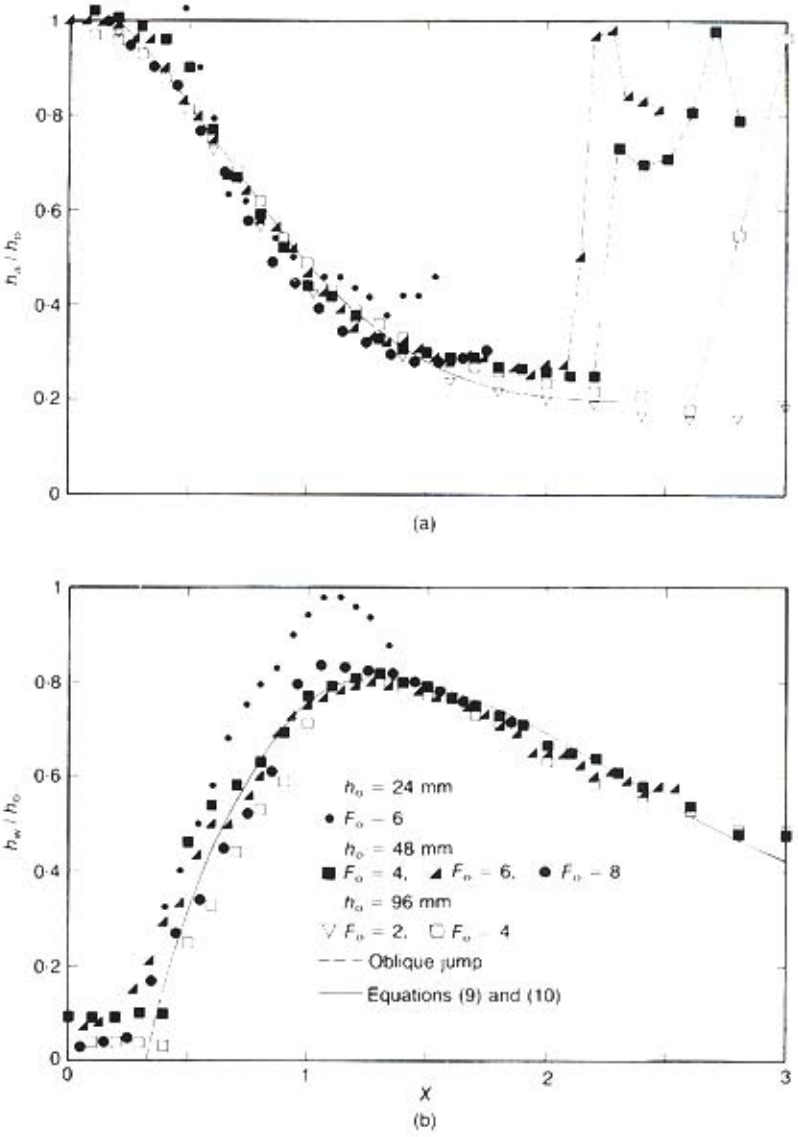

Fig. 7. Longitudinal surface profiles along: (a) channel axis $Y_a(X)$; (b) side wall $Y_w(X)$

is the shock profile recommended for prototype structures, which follows the data for $F_o = 2$, $h_o = 96$ mm. The *expanding* border curve is almost straight and may be expressed as

$$Y_s = 0{\cdot}8 + 6X, \quad 1{\cdot}2 < Y_s < 2{\cdot}8 \qquad (12)$$

The first reflection point is located at $X_s \cong 0{\cdot}4$, and the next part of the shock profile has an initial slope $dY_s/dX = -0{\cdot}75$. Its virtual origin is located at $X = 0{\cdot}25$, and the shock front may be approximated as

$$3 - Y_s = -0{\cdot}25 + 0{\cdot}75X + 0{\cdot}07X^2, \quad 0{\cdot}5 < X < 3{\cdot}3 \qquad (13)$$

The non-linear effect in the far field is thus revealed, as the number 0·07 is, in general, a function of approach Reynolds number.

Effect of expansion ratio

33. The effect of expansion ratio was studied with additional experiments involving

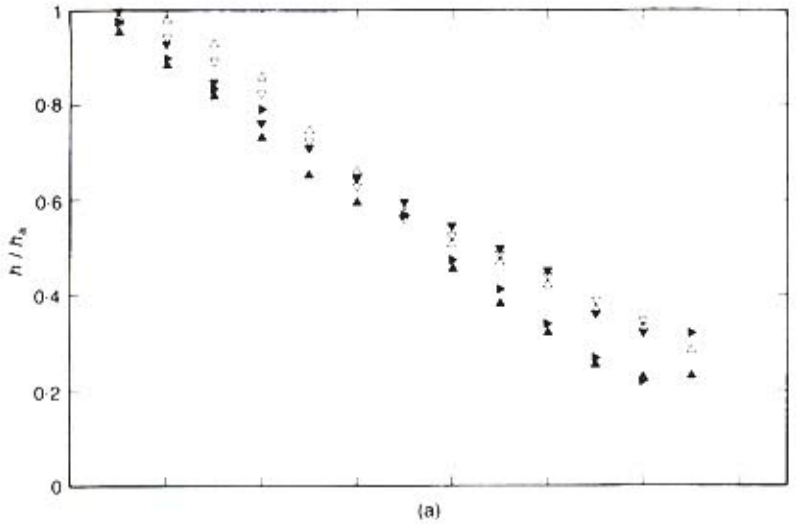

(a)

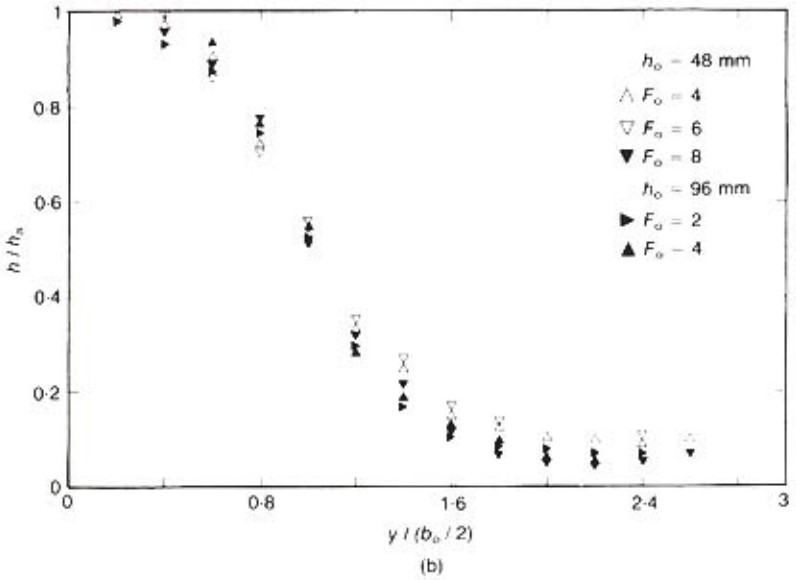

(b)

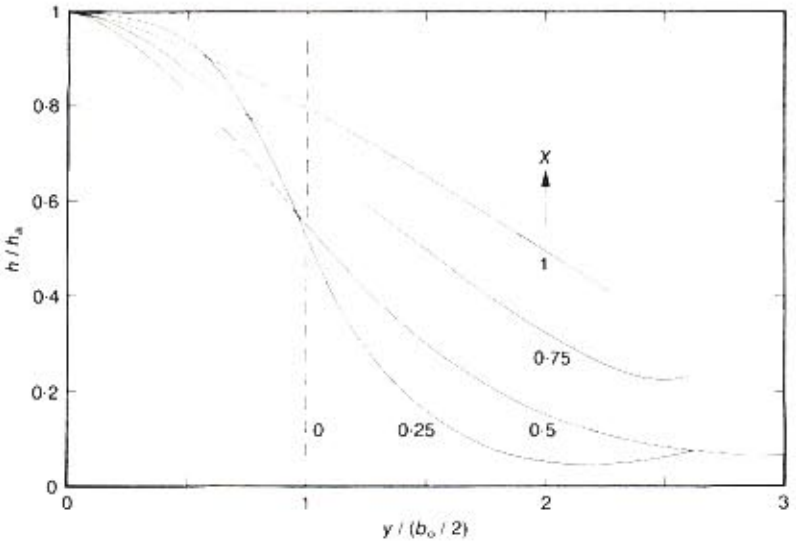

an approach flow depth $h_o = 48$ mm. For $\beta = b_2/b_o = 2$, the original approach width was kept as $b_o = 0{\cdot}50$ m, as for the series with $\beta = 3$, but two aluminium walls were fixed on the existing tailwater channel bottom with $b_2 = 1{\cdot}0$ m. This channel was therefore a full model of comparable size. As regards the width ratio $\beta = 5$, the approach channel was divided with an aluminium wall to yield a half model of width $b_o/2 = 0{\cdot}125$ m. The width of the tailwater channel thus became $b_o/2 = 0{\cdot}626$ m.

34. The *axial surface profile* $Y_a = h_a/h_o$ as a function of $X = (x/b_o)\boldsymbol{F}_o^{-1}$ is shown in Fig. 12(a), together with equation (9), which may be considered independent from the width ratio β, provided that the domain beyond the first shock is excluded. The data at $X \simeq 0$ is somewhat higher than $Y_a = 1$ because of increasing flow depth resulting from wall friction from the gate outlet at location $x = -0{\cdot}8$ m to the expansion section ($x = 0$).

35. The *wall surface profile* $Y_w = h_w/h_o$ is plotted in Fig. 12(b). An effect of expansion ratio may now be seen, but the effect of $\boldsymbol{F}_o$ is again negligible. Generalizing the parameter τ as

$$\tau = \frac{X - X_m}{X_M - X_m} \tag{14}$$

with

$$X_m = \tfrac{1}{6}(\beta - 1) \tag{15}$$

$$X_M = 0{\cdot}52\beta^{0{\cdot}86} \tag{16}$$

as minimum and maximum locations of wall depth height, and

$$Y_{wM} = 1{\cdot}27\beta^{-0{\cdot}4} \tag{17}$$

as maximum wall depth for $1{\cdot}8 < \beta < 6$, the profile of wall depth may be expressed as

$$Y_w = Y_{wM}\,\tau \exp(1 - \tau) \tag{18}$$

For $\tau = 3$, equation (18) simplifies to equation (10). Note that the rising curve portion has been approximated slightly below the data, as this trend may also be seen in Fig. 7(b) for $h_o = 96$ mm. Scale effects are therefore removed artificially to some extent.

36. Figure 9 was compared with the data pertaining to $\beta = 2$ and $\beta = 5$, and a reasonable overall agreement existed. Accordingly, the average transverse profiles may be used for $1{\cdot}8 < \beta < 6$.

Fig. 8 (top). Transverse surface profiles h/h_a as a function of $y/(b_o/2)$ for: (a) $X = 0{\cdot}25$; (b) $X = 0{\cdot}75$

Fig. 9 (bottom). Average transverse surface profiles: $Y_T[y/(b_o/2)]$ for various values of X

37. Figure 13 compares the locations of shock front for $\beta = 2$ and $\beta = 5$, with the average curve according to Fig. 11 for $\beta = 3$. The curves for $\beta = 3$ and $\beta = 5$ are seen to collapse in the domain $0{\cdot}8 < X < 2{\cdot}8$ incidentally, while the curve for $\beta = 2$ has another course. Note the small effect of F_o for the latter.

Characterization of flow

38. In order to compare the overall flow pattern of flows in various expansion geometries, the following parameters were introduced by which the smoothness of flow can be measured.

(*a*) *Standard deviation* σ of depth distribution

$$\sigma = \left[\frac{1}{n}\sum_{n}\left(1 - \frac{h}{\bar{h}}\right)^2\right]^{1/2} \tag{19}$$

where $\bar{h}$ is the mean depth, h is the actual depth in a particular cross-section, and n is the number of depth readings per section. For $\sigma = 0$, constant flow depth occurs in a cross-section.

(*b*) *Coriolis coefficient* α indicating the non-uniformity of kinetic energy distribution at a section

$$\alpha = \frac{1}{A\bar{V}^3}\sum_{n} V^2 u \Delta A \tag{20}$$

where V is the absolute local value of velocity, $\bar{V}$ is the cross-sectional average, u is the streamwise component, and ΔA is an elementary area of cross-section; $\alpha = 1$ indicates a uniform velocity distribution.

(*c*) *Waviness factor* W_f as an indication of actual surface width S in a cross-section relative to the channel width b, as

$$W_f = \sum_{n}\left[\frac{1}{\Delta y}(h_i - h_{i-1})\right]^2 \tag{21}$$

where h_i is the flow depth at location $y = i\Delta y$. For $W_f = 0$, the surface is horizontal.

(*d*) *Lateral momentum transfer factor* T_f as the cross-sectional ratio of lateral to longitudinal momentum

$$T_f = \sum_{n} vu\Delta A \Big/ \sum_{n} u^2 \Delta A \tag{22}$$

where (u, v) are the transverse and streamwise velocity components.

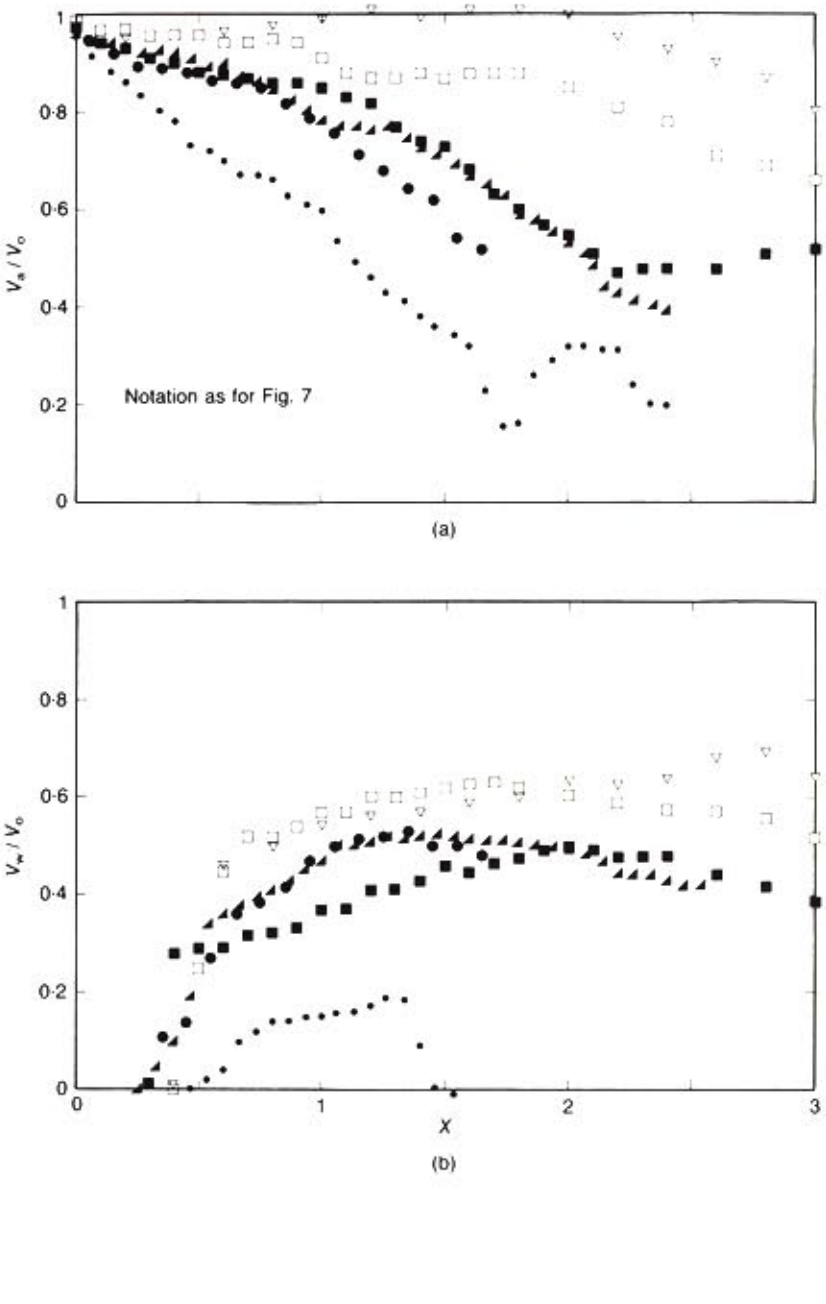

Fig. 10 (top). Longitudinal velocity profiles along: (a) channel axis; (b) channel wall

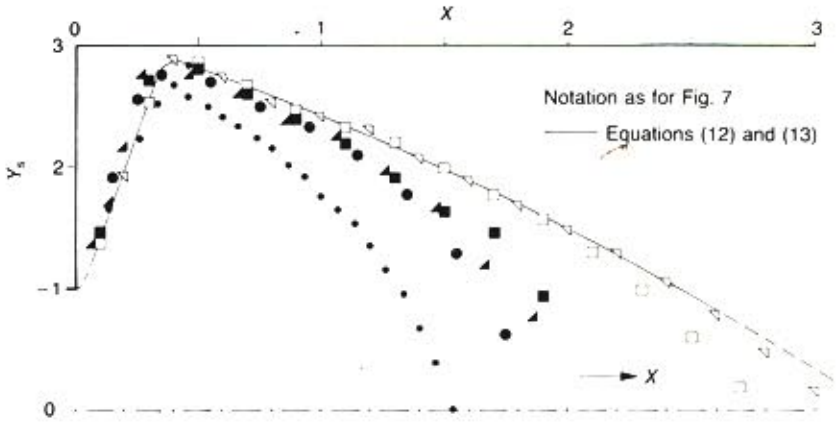

Fig. 11 (bottom). Shock wave pattern $Y_s(X)$ for various runs

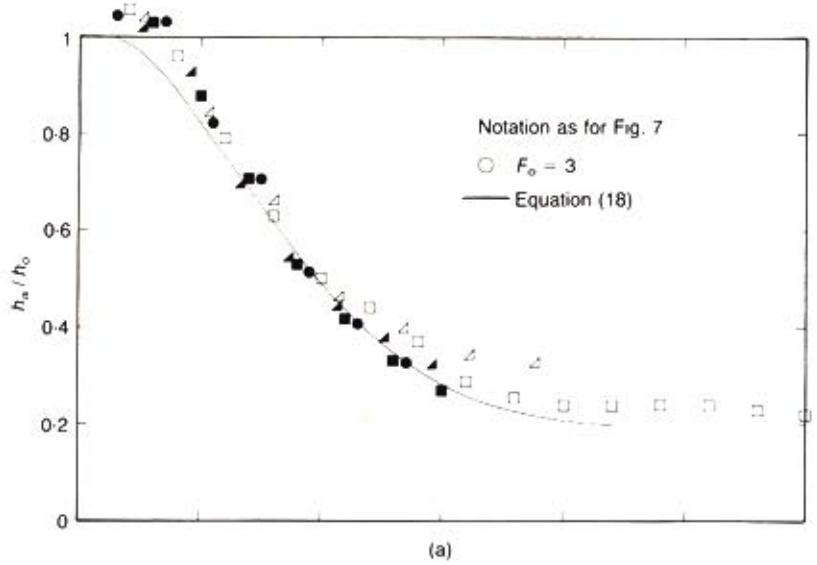

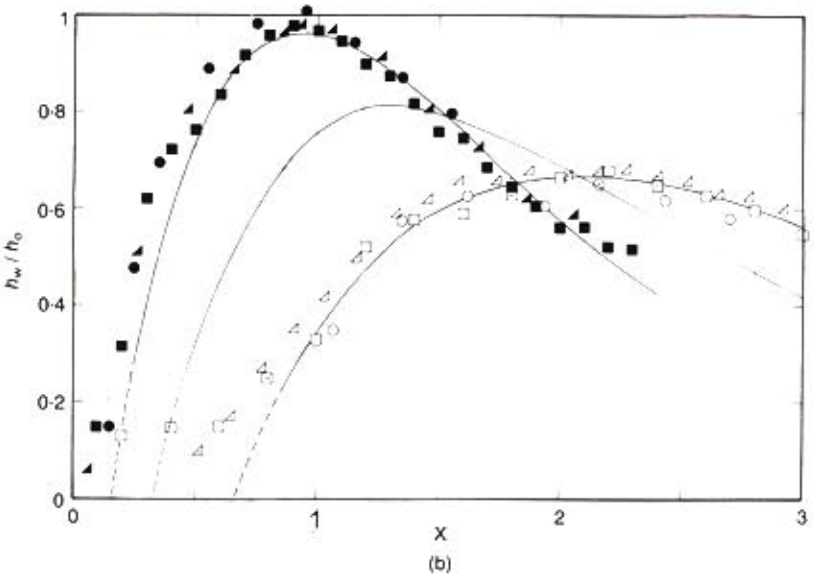

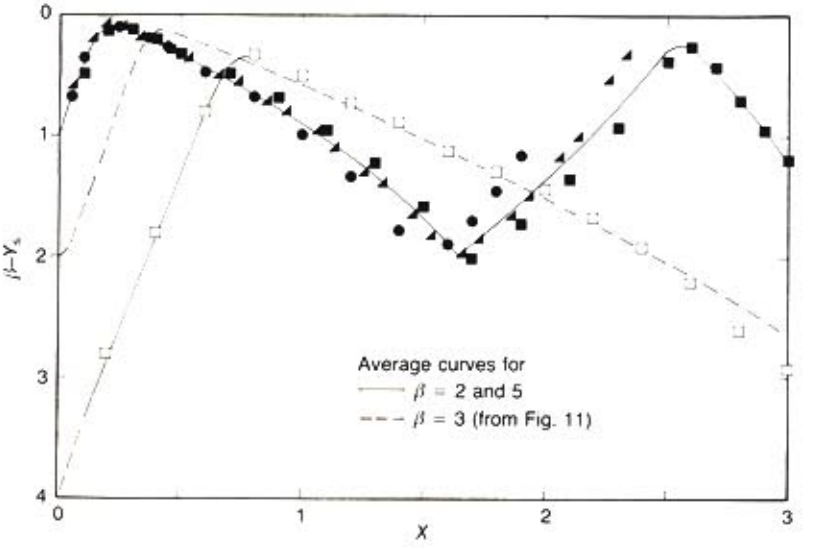

39. Figure 14 shows the *average* cross-sectional flow depth $\bar{h}/h_o$ as a function of X for $\beta = 3$, and reasonable similarity is seen for both $h_o = 48$ mm and $h_o = 96$ mm. The latter may be considered as almost unaffected by scale effects. Note that the relation $\bar{h}/h_o = 0{\cdot}401$ is valid to within $\pm 0{\cdot}03$ in the domain $0 \leqslant X \leqslant 3$.

40. In Fig. 15(a), the *standard deviation* $\sigma(X)$ is plotted. The similarity seems to be preserved also for a constant approach flow depth, independent of $\boldsymbol{F}_o$. For $X > 0{\cdot}7$, the standard deviation is $\sigma < 0{\cdot}5$ and much higher uniformity of flow occurs than close to the expansion section.

41. In Fig. 15(b), the *Coriolis coefficient* $\alpha(X)$ is plotted. There is a general trend visible, with a maximum of $\alpha = 1{\cdot}25 \pm 0{\cdot}05$ at location $X = 0{\cdot}7$, i.e. where full expansion of flow has occurred. Further downstream, α decays to a final value of 1·02–1·04, until the point where reflections occur again on the wall (not shown as $X > 3$).

42. Also included in Fig. 15(b) is the *waviness factor* $W_f(X)$. Similarity is well preserved for the data with $h_o = 48$ mm, while considerable scatter occurs for $h_o = 96$ mm. In general, the waviness factor is below 5%, except for locations close to the expansion section.

Conclusions

43. Based on an experimental study, the flow features in a horizontal abrupt channel expansion are explored for supercritical approach flow with $2 \leqslant \boldsymbol{F}_o \leqslant 8$. The flow pattern is extensively described, and particularities such as the shock front, the expanding flow portion and the reflection mechanism are discussed.

44. Particular attention is paid to the non-dimensional analysis of flow, involving the Rouse streamwise coordinate $X = (x/b_o)\boldsymbol{F}_o^{-1}$. It is shown that both the axial and wall flow depth profiles follow distinct curves of X, provided that effects of scale are insignificant. The dominant scale effect is attributed to viscosity, and thus to the Reynolds number. All relations involving velocity are shown to be strongly governed by scale effects, such that a simple generalization of results is impossible.

45. Further, the transverse surface profiles may be plotted as shown in Fig. 8, and Fig. 11 refers to a generalized plot of shock front geometry. The previous results are then extended to include expansion ratios $2 \leqslant \beta \leqslant 5$.

Fig. 12 (top). (a) Axial and (b) wall surface profiles for $\beta = 2$ (solid symbols) and $\beta = 5$ (light symbols)

Fig. 13 (bottom). Shock fronts for $\beta = 2$ (solid symbols) and $\beta = 5$ (light symbols)

It is shown that both the axial and transverse profiles are independent of β. The wall surface profile involves a significant effect of expansion ratio, as shown in Fig. 12(b). Particular attention should be given to the maximum wall depth Y_{wM} at location X_M as given in equations (16) and (17).

46. In order to compare the flow in abrupt expansions with other expansion geometries, various parameters that characterize the flow have been introduced. These show a high degree of non-uniformity at the expansion domain which may be unacceptable, in which case a geometry other than the abrupt expansion geometry should be chosen.

Acknowledgements

47. The Authors thank Professor R. Sinniger, Director of Laboratoire de Constructions Hydrauliques at EPFL, for his generous support and interest in this study. The help of Mr K. Essyad is also kindly acknowledged.

References

1. Rouse H., Bhootha B. V. and Hsu E.-Y. Design of channel expansions. *Trans. Am. Soc. Civ. Engrs*, 1951, **116**, 1369–1385.
2. Guenzel W. (Wittmann H. (ed.)). *Die schiessende Strahlausbreitung auf geneigter Ebene*. T.-Rehbock Flussbaulaboratorium, Technische Hochschule Karlsruhe, Karlsruhe, 1962, Arbeit **149** (in German).
3. Sherenkov I. A. Solution by computers of the plane problem of the supercritical turbulent flows movement. *XI Int. Association for Hydraulic Research Congr., Leningrad*, 1965, **1**, 3, 1–10.
4. Koch K. (Hartung F. (ed.)). *Die gegenseitige Strahlablenkung auf horizontaler Sohle*. Versuchsanstalt für Wasserbau, TH München, München, 1968, Bericht **15** (in German).
5. Engelund F. *Steady supercritical flow down an inclined plane*. Institute of Hydrodynamics and Hydraulic Engineering, Technical University Denmark, Lingby, 1979, Progress report **48**, 25–30.
6. Bellos C. V., Soulis J. V. and Sakkas J. G. Computation of two-dimensional dam-break-induced flows. *Adv. Wat. Resour.*, 1991, **14**, 1, 31–41.
7. Bremen R. *Expanding stilling basin*. Swiss Federal Institute of Technology, Lausanne (EFPL), 1990, Thesis 850. Also appeared as *Communication* **3**. (Sinniger R. (ed.)). Laboratoire de Constructions Hydrauliques, Dép. de Génie Civil, EPFL, Lausanne.

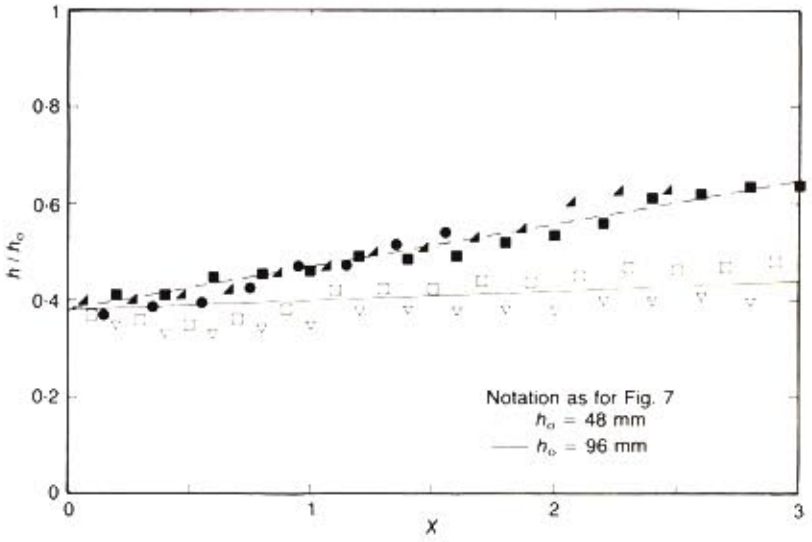

Fig. 14 (top). Average flow depth $\bar{h}/h_o$ as a function of X

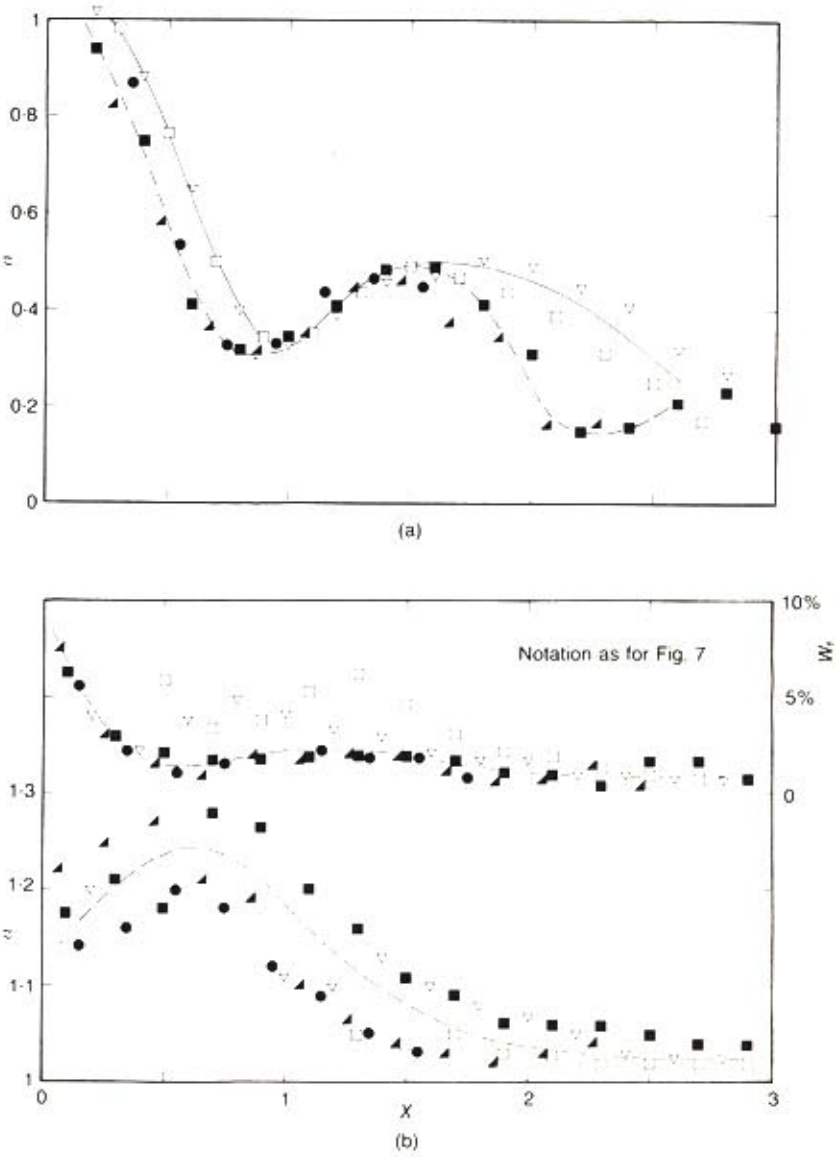

Fig. 15 (bottom). (a) Standard deviation $\sigma(X)$; (b) Coriolis coefficient $\alpha(X)$ (bottom), and waviness factor $W_f(X)$ (top)

8. HAGER W. H., SCHWALT M., CHAUDHRY M. H. and JIMENEZ O. Flow pattern downstream of abrupt wall deflection. *J. Hydraul. Res.* (to be published).
9. ELLIS J. and PENDER G. Chute spillway design calculations. *Proc. Instn Civ. Engrs*, Part 2, 1982, **73**, June, 299–312.
1 IPPEN A. T. and HARLEMAN D. R. F. Verification of theory for oblique standing waves. *Trans. Am. Soc. Civ. Engrs*, 1956, **121**, 678–694.

Bibliography

11. GERNDT R. D. (BORKENSTEIN (ed.)). *Beitrag zur Untersuchung der Bewegungsvorgänge in Tosbecken mit geradliniger, allmählicher Erweiterung*. Institut Wasserbau, Technische Universität Aachen, Aachen, 1971, Mitteilung 3 (in German).